The Faraday Shields Loss of Transformers

Shen, Zhan; Kaymak, Murat; Wang, Huai; Hu, Jingxin; Jin, Long; Blaabjerg, Frede; Doncker, Rik W. de

Published in:
I E E E Transactions on Power Electronics

DOI (link to publication from Publisher):
10.1109/TPEL.2020.2982447

Publication date:
2020

Document Version
Accepted author manuscript, peer reviewed version

The Faraday Shields Loss of Transformers

Zhan Shen, *Student Member, IEEE*, Murat Kaymak, *Student Member, IEEE*, Huai Wang, *Senior Member, IEEE*, Jingxin Hu, *Member, IEEE*, Long Jin, Frede Blaabjerg, *Fellow, IEEE*, and Rik W. De Doncker, *Fellow, IEEE*

***Abstract*— Faraday shields are widely used in high-frequency transformers to conduct the common-mode (CM) current to the ground. They are normally located in the high magnetomotive force (MMF) region, where severe eddy currents are induced and contribute considerable magnetic field losses. In this paper, an analytical procedure is presented for the magnetically-induced loss in Faraday shields. It is originally derived from shields of foil conductors. Then it is extended to different shields with round and Litz wire, and different configurations, e.g., multi-layer shields, interleaved windings, and coaxial transformers. It is verified by the finite element method (FEM) and experimental results in six case studies. Moreover, the criteria to determine the losses of Faraday shields is given and a design procedure is presented to reduce the shield losses at a certain level while keeping the functionality. Finally, a case study is provided to verify the shield design procedure on a 100 kHz transformer.**

***Index Terms*—Common-mode (CM) current, Faraday shield, eddy current, winding losses, isolation transformer.**

I. Introduction

The high-frequency common-mode (CM) noise comes from the fast switching devices and affects the cost and performance of power electronic converters. A Faraday shield conducts the CM current to the ground, and provide galvanic isolation functions [1, 2], as depicted in Fig. 1(a). It is open-circuited, grounded, and located between primary and secondary. The inter-winding capacitance C_{12} is replaced by the capacitance between the Faraday shield and windings, C_{1f} and C_{2f}, respectively, as in Fig. 1(b), (c), and (d). So, the capacitive coupling between the primary and secondary is significantly reduced. The Faraday shield is widely used in sensitive electronics such as audio circuits, electric vehicles [3, 4], PV systems [5], and high-frequency transformers in converters [6–10].

Zhan Shen and Long Jin are with the College of Electrical Engineering, Southeast University, Nanjing 210096, China (e-mail: zhan_shen@seu.edu.cn and jinlong@seu.edu.cn).

Zhan Shen, Huai Wang, and Frede Blaabjerg are with the Center of Reliable Power Electronics (CORPE), Department of Energy Technology, Aalborg University, Aalborg 9220, Denmark (e-mail: zhs@et.aau.dk, hwa@et.aau.dk, and fbl@et.aau.dk).

Murat Kaymak, Jingxin Hu, and Rik W. De Doncker are with the Institute for Power Generation and Storage Systems, E.ON Energy Research Center, RWTH Aachen University, Aachen 52062, Germany (e-mail: mkaymak@eonerc.rwth-aachen.de, jhu@eonerc.rwth-aachen.de, and post_pgs@eonerc.rwth-aachen.de).

There are two kinds of losses in the Faraday shield, i.e., the CM current loss and the magnetically-induced loss. The first one results from the CM current. The CM current also generates the dielectric loss in the insulation material. Both of them are normally neglected, as discussed in Section IV. The magnetically-induced loss is from eddy currents induced by the magnetic field from the windings. It is purely ac resistive loss modeled by the ac resistance, and is the focus of this paper. It also represents the loss of the shield in this paper unless clarified.

The analytical models of the windings loss have been well established in the past. Dowell first derived the closed-form expression for transformer windings in the Cartesian coordinate system [11]. It is widely applied for the winding resistance calculation and optimization [12–14]. Another model is proposed by Ferreira in [15] for round wires and later extended to other kinds of wires. The loss models for Litz wire are proposed in [16–18]. Moreover, the numerical computation method provides more accurate results than one-dimensional formulas and is also adopted for fast resistance calculation [19] and analytical formula parameters acquisition and modification [20, 21].

For the loss of the shield, Lu *et al.* in [3, 9] analyze the shield loss in both planar and coaxial transformers by simulations and experiments. For the analytical approach, a generic formula is proposed for the winding loss of power electronic currents with a broad spectrum, and is extended to the shield [22]. The shield losses in both sinusoidal and half duty cycle full-rectangle-wave magnetic fields are analyzed, and the normalized results are presented. It uses the field harmonic analysis to obtain the magnetomotive force (MMF) as the formula input, unlike Dowell's equation using current directly. It requires the knowledge of magnetic field analysis. When the Fourier analysis of the harmonic current is feasible, using Dowell's equation in each frequency and sum up the loss is also accurate and more accessible [23]. Moreover, the experimental comparison is missing, and the accuracy of the equation is under verification. In [24], the maximum shield thickness is provided on a map that allows a 10% increase of the winding loss under different frequency and winding material. But no analytical equation is presented.

This paper studies the loss of the Faraday shields with three major contributions:

1) A generic analytical formula for the shield loss is presented by extending the formula in [22] to different shields, e.g., the round wire, foil, and Litz wire; different winding configurations, e.g., the multi-layer shields, non-interleaved, and interleaved winding; and different types of transformers, e.g., coaxial transformer.

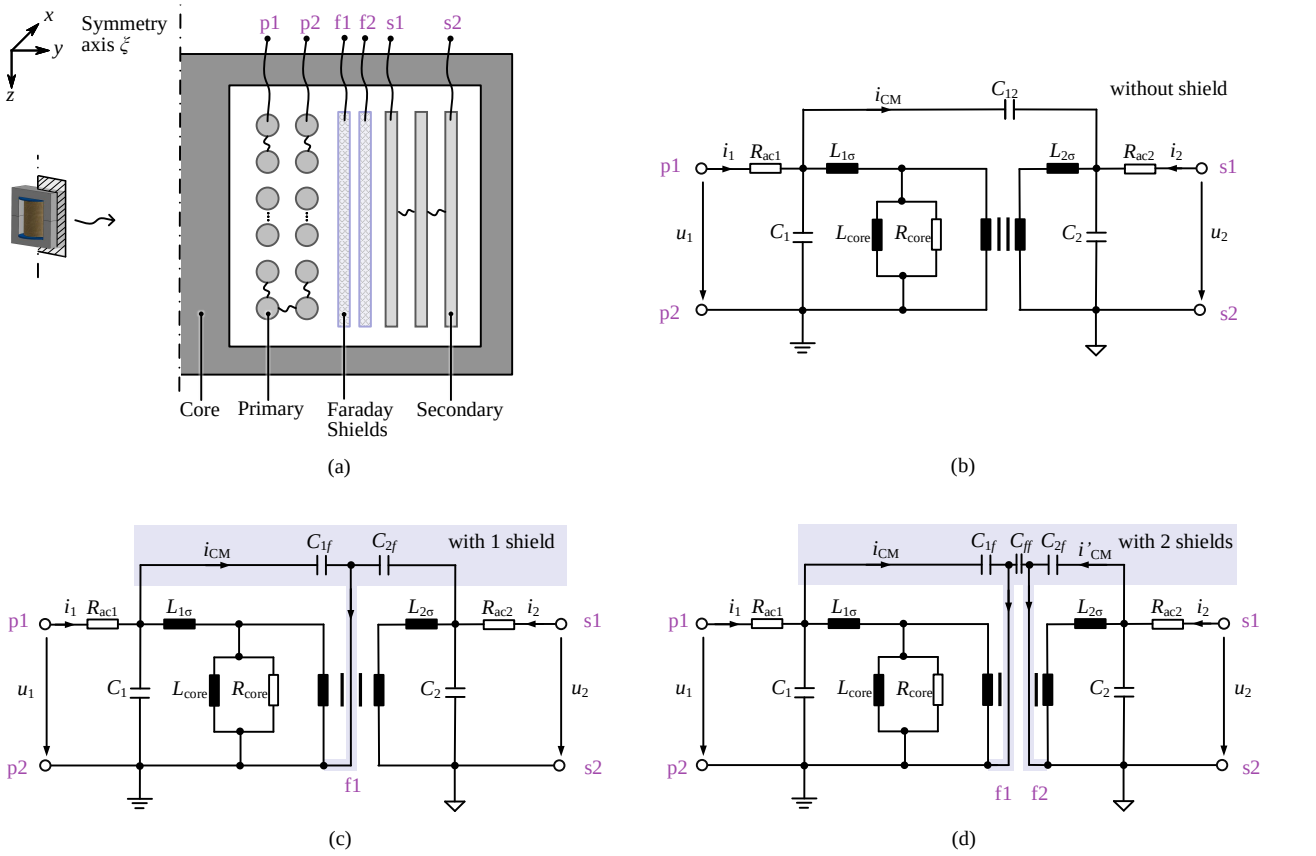

Fig. 1. The cross-section and equivalent circuit of a transformer with and without Faraday shields. (a) is the cross-section of an ETD core transformer with Faraday shields between the primary and secondary windings. (b), (c), and (d) are the equivalent circuit of the transformer without, with 1 and 2 Faraday shields, respectively. p1, p2, f1, f2, s1, s2 are the winding terminals of the primary, shield, and secondary, respectively. For the one shield case (c), the shield is usually connected with p1/p2 in primary or s1/s2 in secondary; for two shields case (d), the shields are connected with p1/p2 and s1/s2, respectively. They conduct the CM current i_{CM} and i'_{CM} to the respective ground. C_{12} is the capacitance between the primary and secondary. By adding the Faraday shield, C_{12} is significantly reduced and replaced by C_{1f}, C_{2f}, and C_{ff}, which are the capacitance between the Faraday shield and the primary, secondary, and the second shield, respectively.

2) The model is verified with finite element method (FEM) simulations and experimental results with six case studies.

3) A design procedure of the Faraday shield is presented. It is verified in a design case study. The criteria to determine the loss of the shields are also presented.

This paper is organized as follows. In Section II, the analytical equation for the Faraday shield loss is presented, followed by a short review of Dowell's equation. The analytical model is applied and verified with different shields by six case studies in Section III. Section IV presents the criteria to determine the shield loss and the procedure to design the shield with a case study. Section V finalizes the paper with the conclusion.

II. Magnetic Field Loss Modeling

A. Winding Resistance without Faraday Shields

In 1966, Dowell derived the closed-form expression for ac resistance of transformer winding $R_{\mathrm{ac}i}$ [11]

$$\begin{aligned} R_{\mathrm{ac}i} &= R_{\mathrm{dc}i}\cdot F_{\mathrm{r}i} \\ &= R_{\mathrm{dc}i}\cdot \triangle_i[\varsigma_i + \frac{2}{3}({p_i}^2-1)\xi_i], \qquad i=1,\ 2 \text{ and } f \end{aligned} \tag{1}$$

where

$$\begin{aligned} R_{\mathrm{dc}i} &= \frac{l_{\mathrm{w}i}\rho_i N_i}{A_i}, & \triangle_i &= \frac{\sqrt{\eta_i}d_{\mathrm{w}i}}{\delta_i}, \\ \eta_i &= \frac{t_i\sqrt{k_i}d_{\mathrm{w}i}}{h_{\mathrm{c}}}, & \delta_i &= \sqrt{\frac{\rho_i}{\pi\mu f}}, \\ \varsigma_i &= \frac{\sinh(2\triangle_i)+\sin(2\triangle_i)}{\cosh(2\triangle_i)-\cos(2\triangle_i)} & \xi_i &= \frac{\sinh\triangle_i-\sin\triangle_i}{\cosh\triangle_i+\cos\triangle_i}, \end{aligned} \tag{2}$$

where $R_{\mathrm{dc}i}$ is the dc resistance, $F_{\mathrm{r}i}$ is the ac resistance ratio, $i=1$, 2, and f stands for the primary, secondary winding, and the Faraday shield, respectively. Further parameter definitions are summarized in Fig. 2.

B. Equivalent Resistance of the Winding with Faraday Shields

In the magnetic field, the skin and proximity effect induce magnetic loss in wires. The skin effect is related to the internal fields induced by the current. Ignoring the CM current, the Faraday shield carries no circuit current. Therefore, it has no skin effect, and the related magnetic field strength is zero

$$H_{\mathrm{intL}f} = -H_{\mathrm{intR}f} = 0 \tag{3}$$

1 2 3 4 5 Five steps for the loss of windings and Faraday shields

- **Subscript 1 : primary winding**
- **Subscript 2 : secondary winding**
- **Subscript f : Faraday shield**

		Primary (i = 1) / Secondary (i = 2)	Faraday Shield ($i = f$)
1.1 **Equiv. thickness d_{wi}, eq.s (2, 8):**	Foil	$d_{wi} = d_i$	$d_{wf} = d_f$
	Round wire	$d_{wi} = \sqrt{\pi} d_i / 2$	$d_{wf} = \sqrt{\pi} d_f / 2$
	Litz wire	$d_{wi} = \sqrt{\pi} d_{stri} / 2$	$d_{wf} = \sqrt{\pi} d_{strf} / 2$
1.2 **Penetration ratio Δ_i, eq. (2):**		$\eta_i = \frac{t_i \sqrt{k_i} d_{wi}}{h_c}$ $\delta_i = \sqrt{\frac{\rho_i}{\pi \mu f}}$ $\triangle_i = \frac{\sqrt{\eta_i} d_{wi}}{\delta_i}$	$\eta_f = \frac{t_f \sqrt{k_f} d_{wf}}{h_c}$ $\delta_f = \sqrt{\frac{\rho_f}{\pi \mu f}}$ $\triangle_f = \frac{\sqrt{\eta_f} d_{wf}}{\delta_f}$
1.3 **Equiv. layers p_i, MMF coefficient α, eq.s (A.6, 7, 9, 10):**	Round wire/ foil, eq. (A.6), Appx. A	$p_i = p_{oi}$ without α	$p_f = 1$ $\alpha = N_1^2$
	Litz wire, eq. (7), Sec. III.B	$p_i = \sqrt{k_i} p_{oi}$ without α	$p_f = \sqrt{k_f}$ $\alpha = N_1^2$
	Multiple shields, Sec. III.D		$p_f > 1$ $\alpha = N_1^2$
	Interleaved, eq. (9,10), Sec. III.E	$p_i = \sum$ without α	$p_f = \sum$ $\alpha = (\frac{N_{pf} I_1 - N_{sf} I_2}{I_1})^2$

- d_1, d_2, d_f : thickness of foil or diameter of round wire
- d_{w1}, d_{w2}, d_{wf} : equivalent thickness
- d_{str1}, d_{str2}, d_{strf} : strand diameter of Litz wire
- k_1, k_2, k_f : number of strands of Litz wire, = 1 for other wires
- p_1, p_2, p_f : equivalent number of layers
- p_{o1}, p_{O2} : original number of layers (bundle level for Litz)
- t_1, t_2, t_f : number of turns per layer
- ρ_1, ρ_2, ρ_f : resistivity of the winding/ shield
- h_1, h_2, h_f : height of the winding/ shield
- η_1, η_2, η_f : porosity factor
- δ_1, δ_2, δ_f : skin depth
- Δ_1, Δ_2, Δ_f : penetration ratio
- l_{wf} : shield mean length per turn
- h_c : height of the core window
- μ : permeability constant
- f : frequency
- N_1 : number of turns of primary
- I_1, I_2 : RMS current in primary/ secondary
- $\sum$: calculate the loss in each layer of the winding/ shield, and sum up
- N_{pf}, N_{sf} : numbers of turns of primary and secondary on the left side of the shield

2&3 Loss of primary (i=1) and secondary (i=2), eq.s (1, 2)

Dc resistance R_{dci}, eq. (2):

$$R_{dci} = \frac{l_{wi} \rho_i N_i}{A_i}$$

Skin effect factor ς_i, eq. (2) :

$$\varsigma_i = \frac{\sinh(2\triangle_i) + \sin(2\triangle_i)}{\cosh(2\triangle_i) - \cos(2\triangle_i)}$$

Proximity effect factor ξ_i, eq. (2) :

$$\xi_i = \frac{\sinh \triangle_i - \sin \triangle_i}{\cosh \triangle_i + \cos \triangle_i}$$

Ac resistance factor F_{ri}, eq. (1):

$$F_{ri} = \triangle_i [\varsigma_i + \frac{2}{3}(p_i^2 - 1)\xi_i]$$

Ac resistance R_{aci}, eq. (1):

$$R_{aci} = R_{dci} \cdot F_{ri}$$

Resistive loss of primary P_{ac1}:

$$P_{ac1} = {I_1}^2 R_{ac1}$$

Resistive loss of secondary P_{ac2}:

$$P_{ac2} = {I_1}^2 \frac{{N_1}^2}{{N_2}^2} R_{ac2}$$

- l_{wi} : mean length per turn
- N_i : number of turns of the winding
- ρ_i : resistivity of the winding
- A_i : cross section area of each turn
- Δ_i : penetration ratio from step 1.2
- p_i : number of layers
- I_i : RMS current in the winding

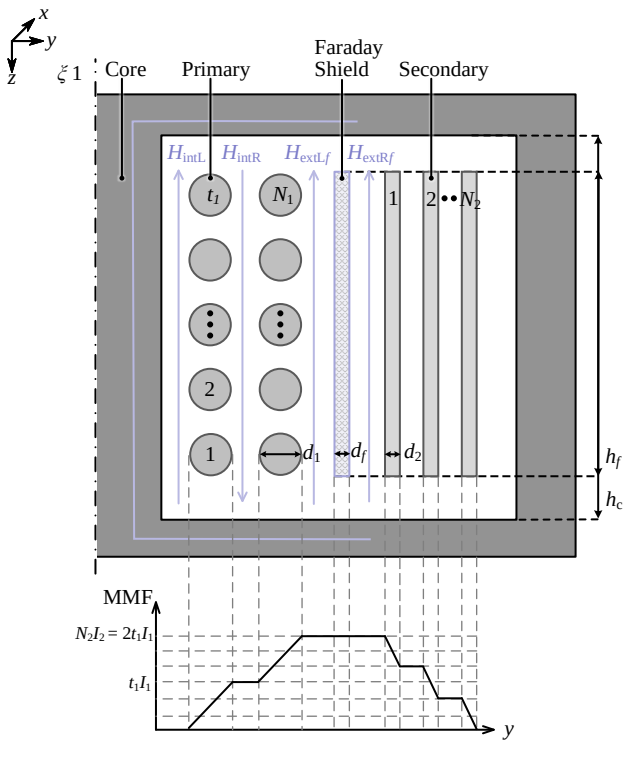

4 Shield loss & resistance converted to primary, eq.s (5) & (A.5)

Proximity effect factor ξ_f, eq. (2) :

$$\xi_f = \frac{\sinh \triangle_f - \sin \triangle_f}{\cosh \triangle_f + \cos \triangle_f}$$

Ac resistance R_{acf}, eq.(5):

$$R_{acf} = p_f \cdot \alpha \frac{2 \triangle_f l_{wf} \rho_f \xi_f}{h_f d_{wf}}$$

Resistive loss P_{acf}, eq.(A.5):

$$P_{acf} = (I_1)^2 p_f \cdot \alpha \frac{2 \triangle_f l_{wf} \rho_f \xi_f}{h_f d_{wf}}$$

- Parameters definitions are in step 1

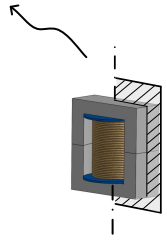

5 Total ac resistance referred to primary

$$R_{ac} = R_{ac1} + R_{acf} + \frac{{N_1}^2}{{N_2}^2} R_{ac2}$$

Primary Shield Secondary

Total winding loss

$$P_{ac} = P_{ac1} + P_{acf} + P_{ac2}$$

Primary Shield Secondary

Fig. 2. Five steps to calculate the ac resistance R_{ac} and loss P_{ac} of windings and the Faraday shield, including the resistances and losses of the primary winding R_{ac1}, P_{ac1} (step 2), secondary winding R_{ac2}, P_{ac2} (step 3), and Faraday shield R_{acf}, P_{acf} (step 4), respectively. The skin effect magnetic field intensity H_{intL} and H_{intR} are with the first layer of the primary winding, and the external proximity effect magnetic field intensity H_{extLf} and H_{extRf} are with the Faraday shield, respectively.

TABLE I
WINDING PARAMETERS OF TRANSFORMERS P1 TO P4

	Pri. Sec. P1∼P4		Faraday shield P1	P2	P3	P4
Shield type				Wire	Litz	Foil
Turns N_i	34	34		34	26	1
Layers p_i	1	1		1	1	1
Dia. d_i (mm)	1.0	1.0		1.0	0.2	0.2
Strands k_f					25	
R_{aci} @ 200 kHz (Ω)			P1	P2	P3	P4
Pri. R_{ac1}			0.28	0.28	0.28	0.28
Sec. R_{ac2}			0.34	0.37	0.39	0.34
Shield R_{acf}				0.66	0.30	0.06

where H_{intLf} and H_{intRf} are the internal magnetic field strengths on the left and right side of the shield, respectively.

The proximity effect is generated by external fields of windings nearby. The Faraday shield locates between the primary and secondary windings with the high magnetomotive force (MMF). Dowell's equation assumes that the field line is one-dimensional, straight, and parallel with the winding in z direction, as in Fig. 2. When applied here, the external magnetic field intensity on the left and right side of the shield are

$$H_{extLf} = H_{extRf} = \frac{N_i \hat{I}_i}{h_c}, \quad i = 1 \text{ for primary and 2 for secondary} \tag{4}$$

where $\hat{I}_i$ is the peak current of the primary or secondary winding. The proximity effect induces the uneven current distribution in wires and leads to ac resistive losses.

Substituting the field intensities into (A.5) in Appendix A, the loss P_{acf} in the Faraday shields is derived as (A.5). (A.5) is also available by extending the general equations with the field analysis method in [22]. P_{acf} is represented as an increment of the ac resistance of the primary side R_{acf}

$$R_{acf} = p_f \cdot \alpha \frac{2 \triangle_f l_{wf} \rho_f \xi_f}{h_f d_{wf}} \tag{5}$$

with the MMF coefficient $\alpha = N_1{}^2$. Other parameters are defined in Fig. 2. Different shield and winding types are considered by changing p_f and α according to Fig. 2 step 1 and Fig. 7. For current with harmonics, the total loss is the sum of P_{acf} at the frequency of its Fourier components.

III. MODEL ANALYSIS AND VERIFICATION: SIX CASE STUDIES

A. Case 1: The Round Wire Faraday Shield

Two transformers without and with round wire Faraday shield are built and compared, named Prototype 1 and 2 (P1 and P2), respectively. The core is ETD 59/31/22 ferrite and is kept the same in the following cases 2, 3, 4, and 5. The height of the core window h_c = 44 mm. The primary, secondary, and round-wire shield are all with the 1.0 mm diameter wire. It makes the penetration ratio $\triangle = 5$ when $f = 200$ kHz. $\triangle$ higher than that leads to severe eddy current loss and increasing error of Dowell's equation and related assumptions.

TABLE II
STEPS TO R_{ac} OF P2 AT 200 KHZ

Step	Item	Pri.($i=1$) / Sec.($i=2$)	Shield ($i=f$)
1.1	d_{wi}	$\frac{\sqrt{\pi}\times 1}{2} = 0.89$	$\frac{\sqrt{\pi}\times 1}{2} = 0.89$
1.2.1	η	$\frac{34\sqrt{1}\times 0.89}{44} = 0.69$	$\frac{34\sqrt{1}\times 0.89}{44} = 0.69$
1.2.2	δ_i	$\sqrt{\frac{1.68\times10^{-8}}{\pi(4\pi\times10^{-7})\times(200\times10^3)}}$ = 0.15	= δ_1 = 0.15
1.2.3	Δ_i	$\frac{\sqrt{0.69}\times 0.89}{0.15} = 4.93$	$\frac{\sqrt{0.69}\times 0.89}{0.15} = 4.93$
1.3.1	p_i	1	1
1.3.2	α		$34^2 = 1156$
2.1	R_{dc1}	$\frac{0.0789\times(1.68\times10^{-8})\times34}{\pi\times(1\times10^{-3}/2)^2}$ = 0.057Ω	
3.1	R_{dc2}	$\frac{0.1040\times(1.68\times10^{-8})\times34}{\pi\times(1\times10^{-3}/2)^2}$ = 0.076Ω	
2.2/3.2/ 4.1	ξ_i	$\frac{\sinh(4.93)-\sin(4.93)}{\cosh(4.93)+\cos(4.93)}$ = 1.01	$\frac{\sinh(4.93)-\sin(4.93)}{\cosh(4.93)+\cos(4.93)}$ = 1.01
2.3/3.3	ς_i	$\frac{\sinh(2\times4.93)+\sin(2\times4.93)}{\cosh(2\times4.93)-\cos(2\times4.93)}$ = 1.00	
2.4/3.4	F_{r1}	$4.93\times[1.00+\frac{2}{3}(1^2-1)\times1.01]$ = 4.93	
2.5	R_{ac1}	0.057×4.93=0.28Ω	
3.5	R_{ac2}	0.076×4.93=0.37Ω	
4.2	R_{acf}		$1\times1156\times\frac{2\times4.93\times0.0914}{34\times0.89\times10^{-3}}\times\frac{(1.68\times10^{-8})\times1.01}{0.89\times10^{-3}}$=0.66
5	R_{ac}	$0.28+\frac{1^2}{1^2}\times0.37$=0.65Ω	0.65+0.66=1.31Ω

The winding configurations and the calculated winding and shield resistance at 200 kHz are given in Table I. A detailed calculation procedure of the winding resistance of P2 at 200 kHz is given in Table II. The parameters and operators in equations follow the orders in Fig. 2. For wire diameter parameters the unit mm is used, others are SI units unless marked.

The analytical, finite element simulation, and experimental results are presented in Fig. 3. The additional loss of the Faraday shields is represented by the resistance increment (5) in the simulation and experiments. The two-dimensional (2D) axisymmetric FEM simulations are performed with the

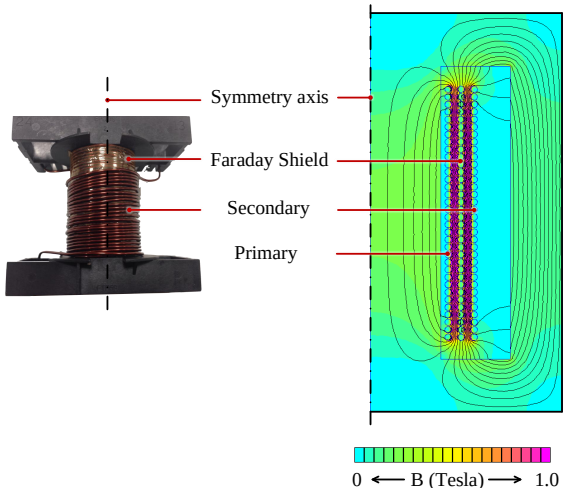

(a)

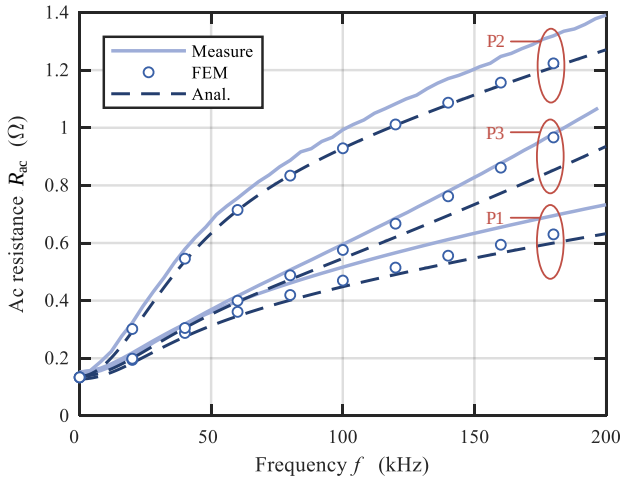

(b)

Fig. 3. (a) Transformer P2 with the round wire shield under construction and its simulation at 200 kHz. (b) The analytical, FEM simulation, and experimental results of transformers without shield (P1), with round wire shield (P2), and with Litz wire shield (P3). The definition of R_{ac} refers to step 5 in Fig. 2.

software FEMM [25]. The measurements are realized with Agilent 4294A Precision Impedance Analyzer.

The analytical, FEM, and measurement results are with the magnetic field in one, two, and three dimensional, respectively. The analytical model assumes the field line is straight and parallel to the shield; the simulation is performed in the two-dimension axisymmetric structure and considers the field distortion; the prototype in reality is not perfectly axisymmetric, and the field distorts in three-dimensional. Their discrepancy due to this reason is called one-dimensional, two-dimensional assumptions, and three-dimensional effect, respectively. The maximum error of the analytical results $R_{ac}(f)_{(Anal.)}$ compared with the measurement $R_{ac}(f)_{(Meas.)}$ is

$$\lambda = \mathrm{MAX}\left| \frac{R_{ac}(f)_{(Anal.)} - R_{ac}(f)_{(Meas.)}}{R_{ac}(f)_{(Meas.)}} \times 100\% \right| \quad (6)$$

It is the maximum error along with the whole measured frequency. λ of P1 and P2 are 16.49% and 13.19%, respectively. The errors result from the one-dimensional field assumption in the analytical model; the two-dimension assumption in the simulation; and the errors in the measurement such as the additional resistance of the leads. In general, the errors are in the acceptable range.

B. Case 2: The Litz Wire Faraday Shield

For Faraday shields with Litz wire, an equivalent transformation is performed referring to [13, 17]

$$p_f = \sqrt{k_f} \quad (7)$$

where k_f is the number of strands, $\sqrt{k_f}$ is the effective number of shield layers. ξ_f for Litz wire is calculated in (2) with

$$d_{wf} = \sqrt{\pi} d_{strf}/2 \quad (8)$$

where d_{strf} is the diameter of the single strand.

Prototype 3 (P3) with the one layer Litz wire shield is built and tested in Fig. 3. The winding configuration is listed in Table I. The maximum analytical error λ of P3 is 10.54%. The FEM simulation is closer to measurement, with a 1.18% error at 180 kHz. This is because the simulation considers the two-dimensional effect. Besides, the Litz wire is with the insulation and twisting effects. The analytical model with (7, 8) does not consider all the skin and proximity effects in strand and bundle level [16].

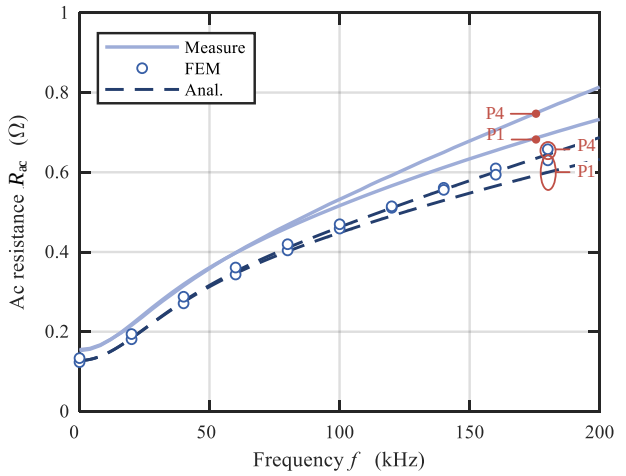

Fig. 4. The analytical, FEM simulation, and experimental results of transformers without shield (P1) and with foil shield (P4).

The round wire shield in Case 1 is with the same copper cross-section area, and the Litz wire is with significantly smaller shield loss. However, it is not guaranteed in other cases. A general method to choose between the single-layer round wire or Litz wire shield is to compare their equivalent resistance directly. If other parameters are the same, when $\sqrt{k_f}\xi_f$ of the Litz ($d_{wf} = \sqrt{\pi} d_{strf}/2$) is smaller than ξ_f of the round wire ($d_{wf} = \sqrt{\pi} d_f/2$), the Litz wire is preferred.

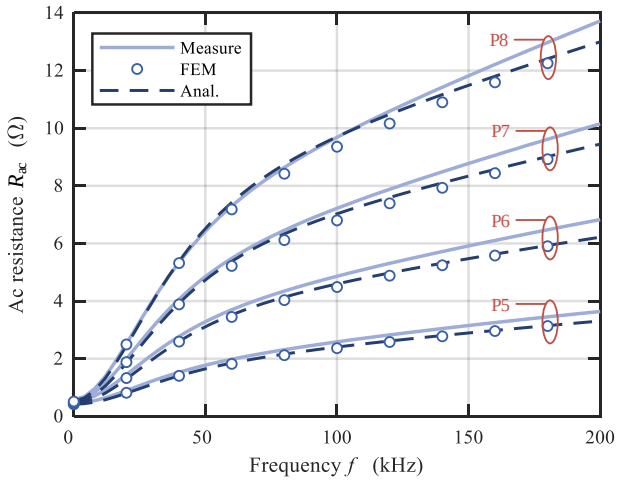

Fig. 5. The analytical, FEM simulation, and experimental results of transformers without shield (P5), with one layer (P6), two layers (P7), and three layers (P8) shields.

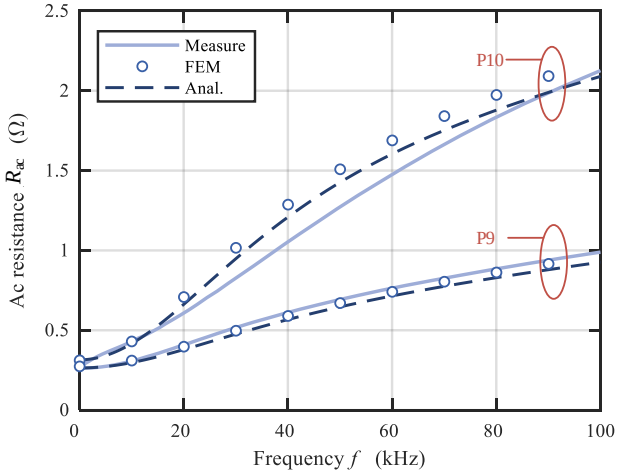

Fig. 6. The analytical, FEM simulation, and experimental results of interleaved transformers without shield (P9) and with shields (P10).

TABLE III
WINDING PARAMETERS OF MULTI-LAYER-SHIELDS TRANSFORMERS P5 TO P8

	Pri.	Sec.	Faraday Shield			
	P5∼P8		P5	P6	P7	P8
Shield layers				1	2	3
Turns N_i	68	34		34	68	102
Layers p_i	2	1		1	2	3
Dia. d_i (mm)	1.0	1.0		1.0	1.0	1.0
R_{aci} @ 200 kHz (Ω)			P5	P6	P7	P8
Pri. R_{ac1}			1.85	1.85	1.85	1.85
Sec. R_{ac2}			0.37	0.40	0.44	0.48
Shield R_{acf}				2.75	5.82	9.21

TABLE IV
WINDING PARAMETERS OF INTERLEAVED TRANSFORMERS P9 AND P10

	Pri.	Sec.	Shields	
	P9∼P10		P9	P10
Shield type			Interleaved	
Turns N_i	68	68		102
Layers p_i	2	2		3
Dia. d_i (mm)	1.0	1.0		1.0
R_{aci} @ 100 kHz (Ω)			P9	P10
Pri. R_{ac1}			0.43	0.43
Sec. R_{ac2}			0.50	0.61
Shield R_{acf}				1.04

C. Case 3: The Foil Faraday Shield

Prototype 4 (P4) with foil Faraday shield is also built and tested (c.f. Fig. 4). The winding parameters are in Table I. The analytical and simulation results of P1 and P4 almost coincide with each other due to the thin shield. The difference between P1 and P4 is only distinct with the increase of frequency. It explains that shield losses are not apparent in some experimental comparisons or applications [9]. The maximum analytical error λ of P4 is 17.65%. It results from the three-dimensional effect which both the analytical and FEM models cannot capture, and the experimental errors, e.g., the measurement error and the additional resistance of the winding leads.

D. Case 4: Multi-layer of Faraday Shields

Double or multi-layer Faraday shields are used in isolation transformers for better CM noise cancellation [26, 27]. The typical connections of the one and two shields scenarios are in Fig. 1. For more shields, their one terminal is normally parallel-connected and grounded with primary/secondary winding, and another terminal is floating. In multi-winding transformers, the windings carrying no current can also behave like multi-layer shields [28].

If p_f layers of shields are placed between the primary and secondary, the magnetic field does not change much because the shields do not provide any current source. Hence, the loss of each shield is the same as (A.5).

Prototypes 5, 6, 7, and 8 (P5∼P8) are built with 0, 1, 2, and 3 layers of shields, respectively. The winding parameters are in Table III. The comparison of ac resistance R_{ac} is in Fig. 5. The maximum analytical errors λ of P5, P6, P7, and P8 are 10.55%, 12.88%, 8.95%, and 7.25%, respectively. The consistency between the analytical, FEM, and measurement results verifies that the field distortion when inserting the shields between windings can be neglected.

E. Case 5: Faraday Shields in Interleaved Transformers

For interleaved transformers, the MMF coefficient α is

$$\alpha = \left(\frac{N_{pf} I_1 - N_{sf} I_2}{I_1}\right)^2 \tag{9}$$

where N_{pf} and N_{sf} are the numbers of turns of primary and secondary on the left side of the shield, I_1 and I_2 are the conducting RMS currents in the primary and secondary,

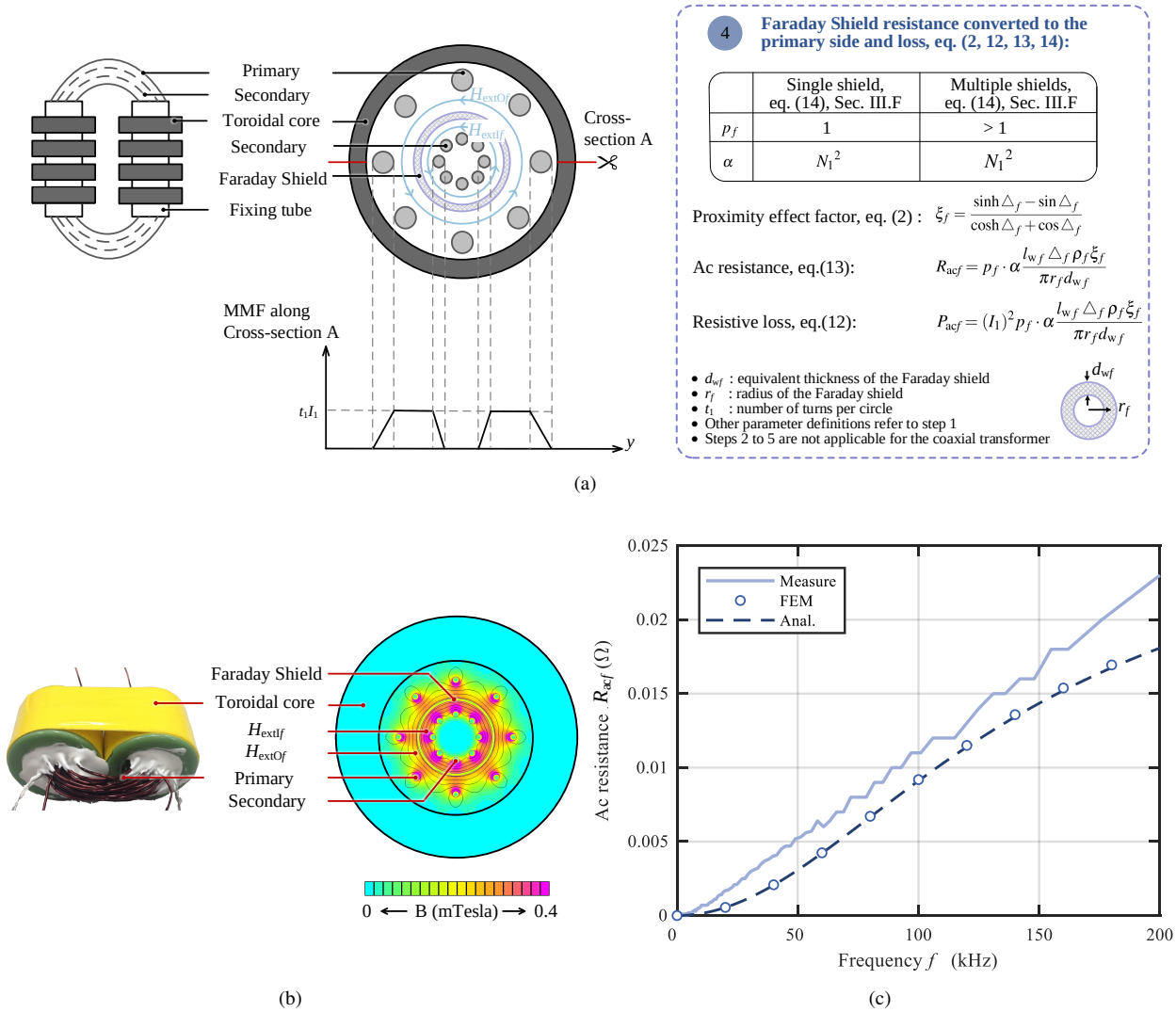

Fig. 7. (a) The top view and cross-section of the coaxial transformer with Faraday shields, formulas of the shield loss. (b) is its magnetostatic simulation at 200 kHz. The magnetic field intensity lines inside the shield H_{extIf} and outside of the shield H_{extOf} are also plotted. (c) is the analytical, FEM simulation, and experimental results of the shield resistance of the coaxial transformer,which is obtained by subtracting the ac resistance of P12 with shield from the ac resistance of P11 without the shield P11.

respectively. The loss in each shield is different, and the total loss is the sum of loses of each shield. Therefore, $\sum$ is used to replace p_f in (5, A.5) to represent this procedure:

$$p_f = \sum \tag{10}$$

Two interleaved transformers Prototypes 9 and 10 (P9 and P10) without and with Faraday shields are built and tested in Fig. 6. The winding parameters are in Table IV. The interleaved layout is *pri.-shield-sec.-shield-pri.-shield-sec.*. The interleaved transformer reduces the maximum magnetic field strength, so the loss in single layer Faraday shield, the ac resistance of the primary and secondary winding, and the leakage inductance decrease. However, the number of shield layers increases. Thus there is a trade-off in terms of loss between the increase of the shield numbers and the decrease of winding and single-layer shield loss.

The maximum analytical errors λ of P9 and P10 are 7.98% and 15.41%, respectively. The analytical and FEM results of P10 are more consistent with each other compared with the measurement, which attributes to the measurement errors and the three-dimensional effect which the analytical and simulation cannot capture.

F. Case 6: Faraday Shields in Coaxial Transformers

The Faraday shield is also used in coaxial transformers as in Fig. 7. There is no net current in the shield, therefore the field intensity at the outer side of the shield H_{extOf} and inner side of the shield H_{extIf} are similar

$$H_{extOf} = \frac{N_i \hat{I}_i}{2\pi(r_f + d_{wf}/2)} \quad H_{extIf} = \frac{N_i \hat{I}_i}{2\pi(r_f - d_{wf}/2)}$$
$$H_{extOf} \approx H_{extIf} \approx \frac{N_i \hat{I}_i}{2\pi r_f} \tag{11}$$

$i = 1$ for the primary and 2 for the secondary

where r_f is the radius from the shield to the center of the core axis, $2\pi r_f$ replaces h_f as the effective magnetic field

TABLE V
WINDING PARAMETERS OF COAXIAL TRANSFORMERS P11 AND P12

	Pri. Sec.	Shields	
	P11∼P12	P11	P12
Shield type			Foil
Turns N_i	8 8		1
Layers p_i	1 1		1
Dia. d_i (mm)	1.0 1.0		0.4
Winding radius r_i (mm)	8.5 3.5		5.1
R_{aci} @ 200 kHz (Ω)		P11	P12
Shield R_{acf}			0.018

length. Usually $r_f \gg d_{wf}$, so the approximation made in (11) is reasonable. The derivation in Appendix A follows Dowell's one-dimensional straight-line magnetic field assumption. It is also applied here for the circle-shaped field, like Dowell's equation for the round wires. Therefore, the shield losses and equivalent resistance referring to the primary side are

$$P_{acf} = (I_1)^2 p_f \cdot \alpha \frac{l_{wf} \triangle_f \rho_f \xi_f}{\pi r_f d_{wf}} \tag{12}$$

$$R_{acf} = p_f \cdot \alpha \frac{l_{wf} \triangle_f \rho_f \xi_f}{\pi r_f d_{wf}} \tag{13}$$

where

$$\alpha = N_1^2 \tag{14}$$

Two coaxial transformers P11 and P12 without and with Faraday shield are built and tested in Fig. 7(b) and (c). Four toroid cores are used for each transformer, with two on each side. The inner, outer diameter, and height of the toroid core are 23, 36, and 16 mm, respectively. The winding configuration is in Table V. The shield is made of copper foil. The FEM and measurement results are obtained by subtracting the ac resistance of P12 and P11.

The coaxial transformer is with the round-circle shaped magnetic field. The solution in the cylindrical-coordinate system is preferred, and the primary and secondary winding resistance with this model is in [29]. It is not presented here due to the limit page and scope of the paper. On the other side, the proposed model is based on Dowell's one-dimensional field assumption and achieves good accuracy here. Above 60 kHz, the maximum analytical error of the shield resistance is 28.43%. Below this frequency, P11 and P12 are with significant large primary and secondary winding resistances compared with the shield equivalent resistance. The errors of their subtraction increase with the decrease of the frequency.

In conclusion, the analytical model in the six cases fit the FEM simulation and measurement in a wide range of frequency. This model follows Dowell's assumption. Therefore, they are with the same character in terms of errors, e.g., the accuracy increases with the increase of the porosity factor.

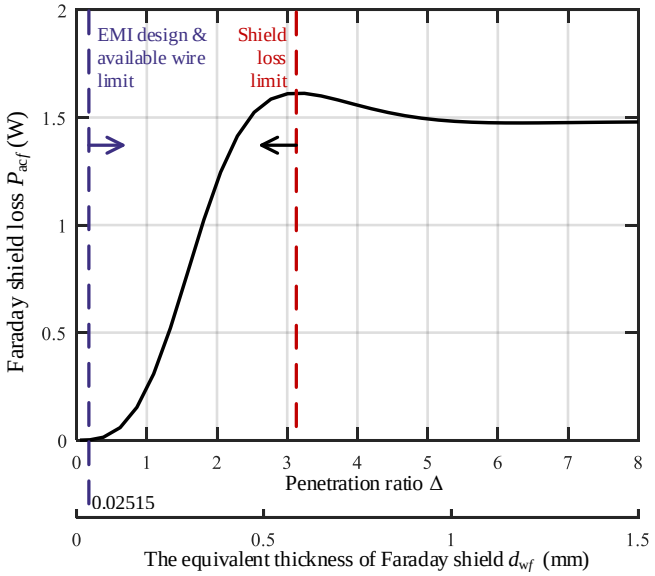

Fig. 8. Determine the optimal shield thickness range based on the shield loss. The loss is calculated with the configurations of transformer P6 with 100kHz, 1A RMS current. d_{wf} is restricted by the EMI function limit to conduct CM current, the shield loss limit, and available wire limit (the thinnest commercial available wire AWG 50, 0.02515 mm).

IV. FARADAY SHIELD DESIGN

A. Design Procedure and the Criteria to Determine Shield Losses

The shield loss P_{acf} of the transformer P6 is illustrated in Fig. 8. It is represented by an ac resistance converted to the primary side R_{acf} in (5). R_{acf} is proportional to $p_f \cdot \xi_{2f}$, which is a function of d_{wf}. So both P_{acf} and R_{acf} increase with d_{wf}, then decrease, and finally keep stable.

To qualitatively decrease the shield losses, there are two methods:

1) Reducing the thickness d_{wf}. Typically d_{wf} is designed below the highest resistance point to reduce the resistive losses, as is illustrated by the shield loss limit with red dashed line. In [28], d_{wf} is suggested below 1/3 of the skin depth.
2) Increasing the conductivity of the shield. It also helps to provide a better electromagnetic interference (EMI) shielding function.

To quantitatively control the shield loss, the shield loss limit in Fig. 8 is used. This limit is to restrict the maximum shield equivalent thickness d_{wf}. In practice, there are two kinds of shield loss limits. The first kind is the maximum loss value $[P_{acf}]_{max}$, which is normally required by each specific design out of the total loss control or thermal considerations. Substituting $[P_{acf}]_{max}$ into (A.5) or (12), the maximum d_{wf} is obtained. The second kind is the shield loss ratio β. It is defined assuming an equal loss of the primary and secondary windings

$$\begin{aligned} \beta &= \frac{P_{acf}}{P_{ac1} + P_{ac2}} \\ &\approx \frac{R_{acf}}{2R_{ac1}} = \frac{m\xi_f}{\varsigma_1 + \frac{2}{3}(p_1{}^2 - 1)\xi_1} = f(p_1, \Delta_1, \Delta_f) \end{aligned} \tag{15}$$

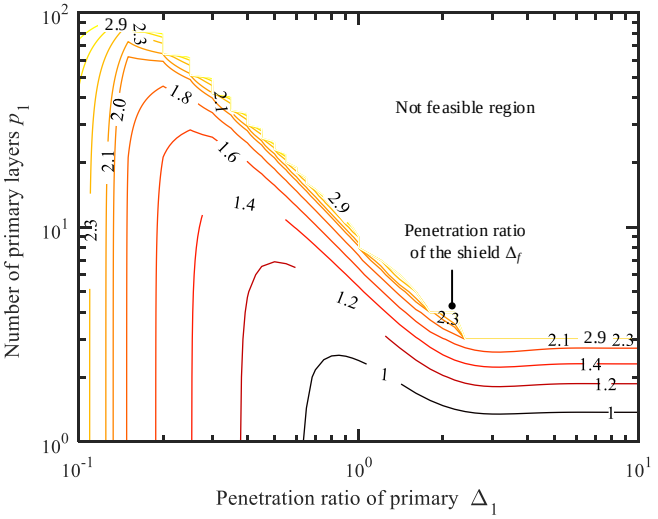

(a)

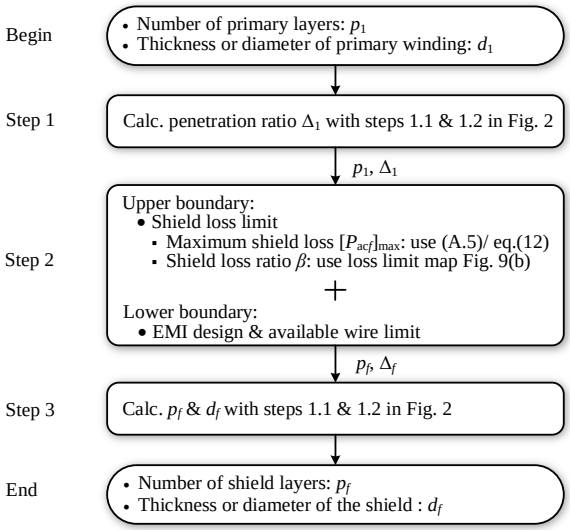

(b)

Fig. 9. (a) The shield loss limit map from eq. (15). With Δ_1 and p_1 from $x-$ and $y-$axes, the indicated value of Δ_f on the contour line is the maximum limit for the shield to keep the shield loss ratio β below 10%. (b) Shield layers and thickness design procedure based on the loss limit map in Fig. 9(a). For an existing design, the calculated d_f is also used for the criteria to determine shield losses.

β is limited to 10% [24]. The shied loss map based on (15) is depicted in Fig. 9(a), while the number of shield layers is p_f =1. From the map, the maximum $\triangle_f$ and d_{wf} are obtained.

The smallest d_{wf} is limited by the EMI design, e.g., the EMI-suppression ability, CM current loss, structure strength requirements, and available smallest diameter of the wires (now it can be as thin as American Wire Gauge (AWG) 50, 0.02515 mm), etc. It is indicated by the blue dashed line in Fig. 8.

In general, there are two boundaries in the shield design. The lower boundary is the EMI design & available wire limit, and the upper boundary is the shield loss limit. Based on that, a design procedure of the shield thickness d_f and number of

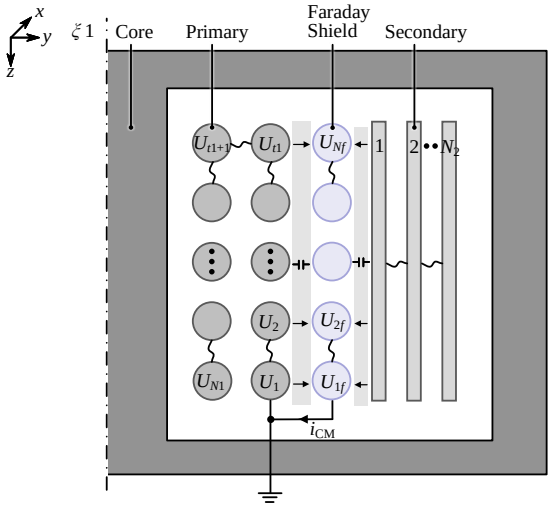

Fig. 10. The common mode (CM) current in the transformer. The connection is the same with Fig. 1(c). U_1, U_2,... U_{N1} are the voltage of each turn in primary, U_{1f}, U_{2f},... U_{Nf} are the voltage of each turn of the shield.

layers p_f is proposed in Fig. 9(b). For an existing design, Fig. 9(b) can be used to determine whether the shield loss should be considered in the modeling.

B. Shield EMI Design

The shield EMI design considers the EMI function limit and the CM current loss. Firstly, the shield should be designed to fulfill EMI regulations such as CISPR-32 [30], which relates to the shield position, grounding/ terminal connection, and shield height/ number of turns. In a standard configuration, a shield is placed between primary and secondary windings with one terminal grounded with primary/ secondary and another terminal floating. Normally, it is made of one turn foil or multi-turns of round wires occupying the whole winding height. Recent advanced techniques modify this standard configuration by performing detailed electrical and magnetic field analysis for each transformer case, which can realize better EMI-suppress functions, as in [2, 31, 32]. The principle of EMI suppression can be simply expressed as Fig. 10. Without the shield, the CM current i_{CM} is induced from the high dv/dt of the switching voltage, flows through the primary, the insulation between windings, secondary, and returns to the ground. When adding a shield, i_{CM} only circulates in the current loops of the primary side (primary winding $\Rightarrow$ insulation $\Rightarrow$ Faraday shield $\Rightarrow$ ground) and secondary side (secondary winding $\Rightarrow$ insulation $\Rightarrow$ Faraday shield $\Rightarrow$ ground) separately. The reduction of the displacement current between the primary and secondary windings leads to a lower EMI level.

Another consideration in the shield EMI design is its CM current losses P_{CMf}. It relates to the shield configuration in the first part and the shield thickness d_f. Usually there is no specific limitation on P_{CMf}, since EMI regulations limit the overall CM current to limit the CM loss and its impact. Therefore, P_{CMf} is only briefly discussed here for completeness. i_{CM} distributively flows from the windings to the shield along the shield height h_f, as Fig. 10. A simplification of the routing

TABLE VI
TRANSFORMER PARAMETERS AND SHIELD DESIGN INPUT

Parameters	Value	
Frequency (kHz)	100	
Core type	PQ 50/50	
Core material	PC44	
Bobbin type	B65982E	
Windings	Pri.	Sec.
Wire type	Litz	Litz
Turns N_i	22	7
Layers p_i	2	1
Dia. d_i (mm)	0.1	0.32
No. of strands k_{str}	350	58

TABLE VII
DESIGN STEPS OF FARADAY SHIELD FOR DAB TRANSFORMER

Step	Item	Calculations
1.1	Equiv. d_{w1}	$\sqrt{\pi}\times 0.1/2 = 0.09$ mm
1.2.1	η_1	$\frac{\frac{22}{2}\times\sqrt{350}\times 0.09}{36.1} = 0.51$
1.2.2	δ_1	$\sqrt{\frac{1.68\times10^{-8}}{\pi(4\pi\times10^{-7})\times(100\times10^{3})}} = 0.21$ mm
1.2.3	$\triangle_1$	$\frac{\sqrt{0.51}\times 0.09}{0.21} = 0.31$
1.3	Equiv. p_1	$\sqrt{350}\times 2 = 37$
2.1	Shield loss map	$\triangle_f \le 2.0$
2.2	EMI & wire limit	$d_f \ge 0.1$, $\triangle_f \ge 0.31$
3	Foil shield design	$p_f = 1, d_f = 0.1$ mm
		$h_f = 32.5$ mm

resistance assumes all i_{CM} flows from the upside floating terminal with U_{Nf} to the downside ground. Considering the foil shield with the cross-section of $d_f l_{wf}$, the shield routing dc resistance R_{dcrt} is

$$R_{dcrt} \approx \rho_f \frac{h_f}{d_f l_{wf}} \tag{16}$$

where ρ_f and l_{wf} are the resistivity and mean length per turn of the shield. The ac resistance R_{acrt} is calculated with Dowell's equation and only considers the skin effect:

$$R_{acrt} = R_{dcrt}\cdot F_{rrt} = R_{dcrt}\cdot \triangle_f \varsigma_f \tag{17}$$

and the CM loss P_{CMf}

$$P_{CMf} = i^2_{CM}\cdot R_{acrt} \tag{18}$$

At fundamental frequency f, $\triangle_f \le 3$ as required by the design map Fig. 9. For harmonics at a higher frequency, e.g., $100f$, $\triangle_{100f} \le 30$, $R_{acrt} \le 30 R_{dcrt}$. i_{CM} is limited by the EMI regulations and with a reduced amplitude as the increase of frequency. It generates CM current loss in the shield with R_{acrt}, and also dielectric loss in the insulation material with R_{insu}. $R_{insu} \gg R_{acrt}$. Usually both CM current and dielectric loss are neglected compared to the magnetically-induced loss which is proportional to the square of the primary current [33].

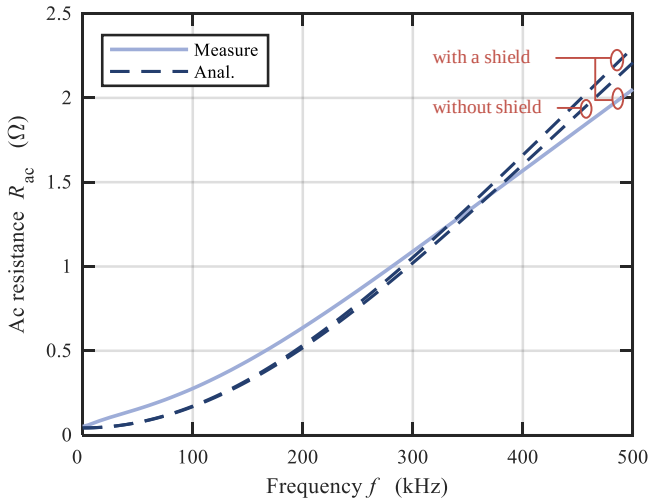

Fig. 11. The analytical and experimental results of the designed transformer without shield and with a shield.

In this work, the EMI design is mainly performed to meet the EMI standards. So, CM currents have no significant effect on the shield design. Depending on the application, if the CM current i_{CM} is not negligible, then the minimum shield thickness d_f can be calculated according to (17) and (18).

C. A Case Study for the Faraday Shield Design

The dual active bridge converter (DAB) is preferred in automotive and renewable energy applications due to its features of high-power density, galvanic isolation, and bidirectional power transfer capability. The Faraday shield is used in its transformer for better isolation and EMI suppression function [4]. In this section, a case study of the shield design in the DAB transformer is presented.

The basic parameters are in Table VI as design input. Three steps are presented in Table VII following the design procedure in Fig. 9. The first step with five sub-steps follows step 1 in Fig. 2. At second step, the shield loss ratio $\beta \le 10\%$ is used as the loss limit. At the calculated point ($\triangle_1 = 0.31, p_1 = 37$) in Fig. 9(a), it is found that $\triangle_f \le 2.0$. In the EMI design, the standard configuration is applied. The shield is between primary and secondary, and connected with the primary ground. The foil shield with the height of 32.5 mm is used to occupy the winding height. There is no CM current shield loss limit. Considering the thinnest foil available in the lab $d_f \ge 0.1$mm, $\triangle_f \ge 0.31$. So $d_f = 0.1$ mm is chosen as the designed shield. The designed transformer is built and tested in Fig. 11, the transformer without shield is also calculated and presented.

The maximum analytical error of the transformer with shield λ is 53.11% @ 35 kHz. The error comes from the mismatch of the assumptions of Dowell's equation for the Litz wire, as discussed in Case 2. Besides, the porosity factor η in this case is low as 0.51. The magnetic field is not parallel with the winding and shield in z-direction, which means severe two-dimensional effect and mismatch of the analytical assumption.

The calculated shield equivalent ac resistance is 3.69 mΩ @ 100 kHz and 87.02 mΩ @ 500 kHz, so the shield loss ratio β of the total ac resistance is 2.14% and 3.84%, respectively. It realizes and verifies the $\beta \leq 10\%$ design target. Since λ is even significantly larger than β, the shield loss in this design is negligible.

V. Conclusions

An analytical expression for ac losses in the Faraday shield based on classical winding loss models is presented. Twelve transformer prototypes related to six case studies on Faraday shields are constructed with different wire types. Both finite element method and experimental results verify the model. The loss of the Faraday shield is not negligible with the increasing number of layers, frequency, and thickness of shields. Finally, the criteria to determine the shield losses and corresponding design procedure are given and verified in a case study. By using the loss limit map, the adequate Faraday shield wire thickness region is derived to maintain the EMI-suppression function and maximum winding loss increase of 10%.

Appendix A
Loss Modeling in Faraday Shields

With the one-dimensional flux distribution and magnetomotive force (MMF) in the winding area, the magnetic field intensity H_z is modeled by the diffusion equation from Maxwell equations

$$\frac{\mathrm{d}^2 H_z}{\mathrm{d}y^2} = j\sigma\omega\mu H_z = \gamma^2 H_z \tag{A.1}$$

where $\gamma = (1+\mathrm{j})/\delta$.

The internal field boundary of the shield refers to (3), and the current distribution for skin effect is

$$J_{\mathrm{s}x} = 0 \tag{A.2}$$

The external field strength of the shield refers to (4). With the identical $H_{\mathrm{extL}f}$ and $H_{\mathrm{extR}f}$, the general solution of (A.1) for proximity effect in z direction is

$$H_{\mathrm{p}z} = \frac{\cosh\gamma y}{\cosh\frac{\gamma d_{\mathrm{w}}}{2}} H_{\mathrm{extL}f} \tag{A.3}$$

The current distribution $J_{\mathrm{p}x}$ for proximity effect is

$$J_{\mathrm{p}x} = \frac{\mathrm{d}H_{\mathrm{p}zf}}{\mathrm{d}y} = \frac{\gamma\sinh\gamma y}{\cosh\frac{\gamma d_{\mathrm{wf}}}{2}} H_{\mathrm{extL}f} \tag{A.4}$$

Substituting $H_{\mathrm{extL}f}$ from (4), the loss of the shield $P_{\mathrm{ac}f}$ is

$$P_{\mathrm{ac}f} = N_f \frac{l_{\mathrm{w}}\rho_f \frac{h_f}{N_f}}{2} \int_0^{d_{\mathrm{wf}}} |J_x|^2 \,\mathrm{d}y = (I_1)^2 p_f \cdot \alpha \frac{2\triangle_f l_{\mathrm{w}f}\rho_f \xi_f}{h_f d_{\mathrm{w}f}} \tag{A.5}$$

where

$$p_f = 1, \qquad \alpha = {N_1}^2, \qquad \xi_{2f} = \frac{\sinh\triangle_f - \sin\triangle_f}{\cosh\triangle_f + \cos\triangle_f} \tag{A.6}$$

References

[1] L. Xie, X. Ruan, Q. Ji, and Z. Ye, "Shielding-cancelation technique for suppressing common-mode EMI in isolated power converters," *IEEE Trans. Ind. Electron.*, vol. 62, no. 5, pp. 2814–2822, May 2015.

[2] C. Fei, Y. Yang, Q. Li, and F. C. Lee, "Shielding technique for planar matrix transformers to suppress common-mode emi noise and improve efficiency," *IEEE Trans. Ind. Electron.*, vol. 65, no. 2, pp. 1263–1272, Feb. 2018.

[3] W. Water and J. Lu, "Shielding analysis of high-frequency coaxial transformers used for electric vehicle on-board charging systems," *IEEE Trans. Magn.*, vol. 49, no. 7, pp. 4005–4008, Jul. 2013.

[4] B. Farhangi and H. A. Toliyat, "Modeling isolation transformer capacitive components in a dual active bridge power conditioner," in *Proc. IEEE ECCE*, Sep. 2013, pp. 5476–5480.

[5] H. L. Jou, W. J. Chiang, and J. C. Wu, "Voltage-mode grid-connected solar inverter with high frequency isolated transformer," in *Proc. IEEE Int. Symp. Ind. Electron.*, Jul. 2009, pp. 1087–1092.

[6] P. Kong, S. Wang, F. C. Lee, and Z. Wang, "Reducing common-mode noise in two-switch forward converter," *IEEE Trans. Power Electron.*, vol. 26, no. 5, pp. 1522–1533, May 2011.

[7] Y. P. Chan, B. M. H. Pong, N. K. Poon, and J. C. P. Liu, "Common-mode noise cancellation by an antiphase winding in multilayer isolated planar transformer," *IEEE Trans. Electromagn. Compat.*, vol. 56, no. 1, pp. 67–73, Feb. 2014.

[8] M. R. Yazdani, H. Farzanehfard, and J. Faiz, "EMI analysis and evaluation of an improved zct flyback converter," *IEEE Trans. Power Electron.*, vol. 26, no. 8, pp. 2326–2334, Aug. 2011.

[9] J. Lu and F. Dawson, "Characterizations of high frequency planar transformer with a novel comb-shaped shield," *IEEE Trans. Magn.*, vol. 47, no. 10, pp. 4493–4496, Oct. 2011.

[10] T. Guillod, F. Krismer, and J. W. Kolar, "Electrical shielding of MV/MF transformers subjected to high dv/dt PWM voltages," in *Proc. IEEE APEC*, Mar. 2017, pp. 2502–2510.

[11] P. Dowell, "Effects of eddy currents in transformer windings," *Proc. Inst. Electr. Eng.*, vol. 113, no. 8, pp. 1387–1394, Aug. 1966.

[12] W. Hurley, E. Gath, and J. Breslin, "Optimizing the AC resistance of multilayer transformer windings with arbitrary current waveforms," *IEEE Trans. Power Electron.*, vol. 15, no. 2, pp. 369–376, Mar. 2000.

[13] M. K. Kazimierczuk, *High-frequency magnetic components*. West Sussex, UK: John Wiley & Sons, 2009.

[14] M. Kaymak, Z. Shen, and R. W. D. Doncker, "Comparison of analytical methods for calculating the AC resistance and leakage inductance of medium-frequency transformers," in *Proc. IEEE Wksh. Contr. Modeling Power Electron.*, Jun. 2016, pp. 1–8.

[15] J. Ferreira, "Appropriate modelling of conductive losses in the design of magnetic components," in *Proc. IEEE Power Electron. Spclst. Conf.*, Jun. 1990, pp. 780–785.

[16] C. Sullivan, "Optimal choice for number of strands in a litz-wire transformer winding," *IEEE Trans. Power Electron.*, vol. 14, no. 2, pp. 283–291, Mar. 1999.

[17] R. Wojda and M. K. Kazimierczuk, "Winding resistance of litz-wire and multi-strand inductors," *IET Power Electron.*, vol. 5, no. 2, pp. 257–268, Feb. 2012.

[18] E. Barrios, A. Ursua, L. Marroyo, and P. Sanchis, "Analytical design methodology for litz-wired high-frequency power transformers," *IEEE Trans. Ind. Electron.*, vol. 62, no. 4, pp. 2103–2113, Apr. 2015.

[19] C. Sullivan, "Computationally efficient winding loss calculation with multiple windings, arbitrary waveforms, and two-dimensional or three-dimensional field geometry," *IEEE Trans. Power Electron.*, vol. 16, no. 1, pp. 142–150, Jan. 2001.

[20] X. Nan and C. R. Sullivan, "Simplified high-accuracy calculation of eddy-current loss in round-wire windings," in *Proc. IEEE Power Electron. Spclst. Conf.*, vol. 2, Jun. 2004, pp. 873–879.

[21] M. Bahmani, T. Thiringer, and H. Ortega, "An accurate pseudoempirical model of winding loss calculation in HF foil and round conductors in switchmode magnetics," *IEEE Trans. Power Electron.*, vol. 29, no. 8, pp. 4231–4246, Aug. 2014.

[22] J.-P. Vandelac and P. Ziogas, "A novel approach for minimizing high-frequency transformer copper losses," *IEEE Trans. Power Electron.*, vol. 3, no. 3, pp. 266–277, Jul. 1988.

[23] J. Muehlethaler, "Modeling and multi-objective optimization of inductive power components," PhD thesis, Zurich, Switzerland: ETH Zurich, 2012.

[24] B. Carsten, "High frequency conductor losses in switchmode magnetics," Corvallis, OR, USA: Bruce Carsten Associates., Tech. Rep., 2013.

[25] D. Meeker, *Finite Element Method Magnetics (FEMM)*. Version 4.2, Jan. 2016.
[26] Y. Yang, D. Huang, F. C. Lee, and Q. Li, "Transformer shielding technique for common mode noise reduction in isolated converters," in *Proc. IEEE ECCE*, Sep. 2013, pp. 4149–4153.
[27] D. F. Knurek, "Reducing EMI in switch mode power supplies," in *Proc. Int. Telecom. Energy Conf.*, Oct. 1988, pp. 411–420.
[28] L. H. Dixon, "Eddy current losses in transformer windings and circuit wiring," Dallas, TX, USA: Texas Instruments, Tech. Rep., 1988.
[29] M. S. Rauls, D. W. Novotny, and D. M. Divan, "Design considerations for high-frequency coaxial winding power transformers," *IEEE Trans Ind Appl*, vol. 29, no. 2, pp. 375–381, Mar. 1993.
[30] *Electromagnetic compatibility of multimedia equipment - emission requirements (CISPR 32)*, International Special Committee on Radio Interference (CISPR), 2015.
[31] D. Fu, S. Wang, P. Kong, F. C. Lee, and D. Huang, "Novel techniques to suppress the common-mode EMI noise caused by transformer parasitic capacitances in dc-dc converters," *IEEE Trans. Ind. Electron.*, vol. 60, no. 11, pp. 4968–4977, Nov. 2013.
[32] Y. Li, H. Zhang, S. Wang, H. Sheng, C. P. Chng, and S. Lakshmikanthan, "Investigating switching transformers for common mode EMI reduction to remove common mode EMI filters and y-capacitors in flyback converters," *IEEE Trans. Emerg. Sel. Topics Power Electron.*, vol. 6, no. 4, pp. 2287–2301, Dec. 2018.
[33] T. Guillod, R. Faerber, D. Rothmund, F. Krismer, C. M. Franck, and J. W. Kolar, "Dielectric losses in dry-type insulation of medium-voltage power electronic converters," *IEEE Trans. Emerg. Sel. Topics Power Electron. Early Access.*, 2019.

Zhan Shen (S'16) received the B.E. degree in electrical engineering and automation from Nanjing University of Aeronautics and Astronautics in 2013, and M.E. degree in electrical engineering from Southeast University in 2016, both in Nanjing, China. He is a Research Assistant at Southeast University, Nanjing, China, and the Center of Reliable Power Electronics (CORPE), Aalborg University, Aalborg, Denmark. He was a Visiting Student and pursued his master thesis at the RWTH Aachen University, Aachen, Germany, from Oct. 2014 to Feb. 2016, and a Visiting Scholar with the Massachusetts Institute of Technology (MIT), Cambridge, MA, USA, from Oct. 2018 to Jan. 2019.

He was with the ABB Corporate Research Center, Beijing, China, in 2016. His research interests include the electromagnetic-thermal-reliability modeling and design of magnetic components in power electronic converters.

Murat Kaymak (S'14) received the B. Sc. and M. Sc. degrees in electrical engineering from RWTH Aachen University, Germany, in 2011 and 2014, respectively. Since April 2015, he has been working toward the Ph.D. degree at the Institute for Power Generation and Storage Systems (PGS), RWTH Aachen University. In 2013, he worked with Kiepe GmbH on gate drive units and siliconcarbide semiconductor modules for power converters. His research interests include the design and modeling of magnetic components for power electronics systems.

Huai Wang (M'12, SM'17) received the B.E. degree in electrical engineering, from Huazhong University of Science and Technology, Wuhan, China, in 2007 and the Ph.D. degree in power electronics, from the City University of Hong Kong, Hong Kong, in 2012. He is currently Professor with the Center of Reliable Power Electronics (CORPE), Department of Energy Technology at Aalborg University, Denmark. He was a Visiting Scientist with the ETH Zurich, Switzerland, from Aug. to Sep. 2014, and with the Massachusetts Institute of Technology (MIT), USA, from Sep. to Nov. 2013. He was with the ABB Corporate Research Center, Switzerland, in 2009. His research addresses the fundamental challenges in modelling and validation of power electronic component failure mechanisms, and application issues in system-level predictability, condition monitoring, circuit architecture, and robustness design.

Dr. Wang received the Richard M. Bass Outstanding Young Power Electronics Engineer Award from the IEEE Power Electronics Society in 2016, and the Green Talents Award from the German Federal Ministry of Education and Research in 2014. He is currently the Chair of IEEE PELS/IAS/IES Chapter in Denmark. He serves as an Associate Editor of IET Electronics Letters, IEEE JOURNAL OF EMERGING AND SELECTED TOPICS IN POWER ELECTRONICS, and IEEE TRANSACTIONS ON POWER ELECTRONICS.

Jingxin Hu (S'16, M'19) received the B.S. degree from Northeastern University, Shenyang, China, in 2010, and the M.Sc. and Dr.-Ing. degrees (summa cum laude) from RWTH Aachen University, Aachen, Germany, in 2013 and 2019, all in electrical engineering. From April 2012 to October 2012, he was an intern research assistant at the ABB Corporate Research Center, Baden-Daettwil, Switzerland. From 2013 to 2014, he worked at the High Power Electronics Laboratory at General Electric Global Research Center, Munich, Germany. Since October 2014, he joined the Institute for Power Generation and Storage System, E.ON Energy Research Center, RWTH Aachen University, Aachen, Germany, as a research associate, where he is currently a post-doc senior scientist. Dr. Hu was the recipient of Second Prize Paper Award of IEEE IPEC (ECCE Asia) in 2018 and STAWAG Dissertation Prize in 2019. His main research interests include power electronics, renewable power generation and dc microgrids.

Long Jin received the master degree in automation, and Ph.D. degree in vibration, concussion, and noises from the Nanjing University of Aeronautics and Astronautics, Nanjing, China, in 1993 and 1997, respectively. He is currently a Professor with the School of Electrical Engineering, Southeast University, Nanjing, China. His current research interests include the design and control of high-power electronics, robotics, and ultrasonic motors.

Frede Blaabjerg (S'86, M'88, SM'97, F'03) was with ABB-Scandia, Randers, Denmark, from 1987 to 1988. From 1988 to 1992, he got the PhD degree in Electrical Engineering at Aalborg University in 1995. He became an Assistant Professor in 1992, an Associate Professor in 1996, and a Full Professor of power electronics and drives in 1998. From 2017 he became a Villum Investigator. He is honoris causa at University Politehnica Timisoara (UPT), Romania and Tallinn Technical University (TTU) in Estonia.

His current research interests include power electronics and its applications such as in wind turbines, PV systems, reliability, harmonics and adjustable speed drives. He has published more than 600 journal papers in the fields of power electronics and its applications. He is the co-author of four monographs and editor of ten books in power electronics and its applications.

He has received 32 IEEE Prize Paper Awards, the IEEE PELS Distinguished Service Award in 2009, the EPE-PEMC Council Award in 2010, the IEEE William E. Newell Power Electronics Award 2014, the Villum Kann Rasmussen Research Award 2014, the Global Energy Prize in 2019 and the 2020 IEEE Edison Medal. He was the Editor-in-Chief of the IEEE TRANSACTIONS ON POWER ELECTRONICS from 2006 to 2012. He has been Distinguished Lecturer for the IEEE Power Electronics Society from 2005 to 2007 and for the IEEE Industry Applications Society from 2010 to 2011 as well as 2017 to 2018. In 2019-2020 he serves a President of IEEE Power Electronics Society. He is Vice-President of the Danish Academy of Technical Sciences too. He is nominated in 2014-2019 by Thomson Reuters to be between the most 250 cited researchers in Engineering in the world.

Rik W. De Doncker (M'87, SM'99, F'01), PhD KULeuven, Belgium. In 1987 he was appointed as Visiting Associate Professor at the University of Wisconsin, Madison. After a short stay as an Adjunct Researcher at IMEC, Leuven, he joined in 1989 General Electric Company CR&D, Schenectady, NY. In 1994, he joined Silicon Power Corporation, Malvern, PA as Vice President of Technology. Since Oct. 1996, he is professor at RWTH Aachen University, Germany, leading the Institute for Power Electronics and Electrical Drives (ISEA). Oct. 2006, he was appointed director of the E.ON Energy Research Center at RWTH, where he also founded the Institute for Power Generation and Storage Systems. He is director of the RWTH CAMPUS Cluster Sustainable Energy and leads the Flexible Electrical Networks (FEN) Research CAMPUS. In 2010, he received an Honorary Doctor Degree from TU Riga, Latvia. 2015 he received RWTH Fellow status at RWTH Aachen University.

1997 he founded the German IEEE Joint IAS-PELS-IES Chapter and the IEEE PELS RWTH Student Chapter. While he was President of IEEE PELS '05-'06, he established ECCE Asia as a cooperation between IEE of Japan, KIPE of Korea, CES of China and PELS. He is recipient of the IAS Outstanding Achievements Award, the IEEE Power Engineering Nari Hingorani Custom Power Award (2008), the 2013 Newell Power Electronics IEEE Technical Field Award, and the 2014 IEEE PELS Harry A. Owen Outstanding Service Award. In 2016 he became member of the German Academy of Science and Technology (ACATECH). 2017 he became Member of the International Advisory Board of French automotive research institute VEDECOM. He is recipient of the 2020 IEEE Medal in Power Engineering.